ADVANCED FUNCTIONAL MATERIALS
www.afm-journal.de

Cellular Polypropylene Piezoelectret for Human Body Energy Harvesting and Health Monitoring

*Nan Wu, Xiaofeng Cheng, Qize Zhong, Junwen Zhong, Wenbo Li, Bo Wang, Bin Hu, and Jun Zhou**

Self-powered and wearable electronics, which are away from the problems of batteries, can provide the sustainable and comfortable interactive service for people. In this work, cellular polypropylene piezoelectret, which is with excellent physical and electrical properties, is utilized to build the human body energy harvesting and self-powered human health monitoring systems. The cellular polypropylene piezoelectret flexible generator can reach a maximum peak power density of ≈52.8 mW m^{-2}. Simultaneously, self-powered human body biological signals detecting sensors are demonstrated to detect the human physiological signals, such as coughing action and arterial pulses. This study strongly indicates the great compatibility and potential applications in human healthy monitoring may pave a new developing way for portable and wearable electronics systems.

1. Introduction

Portable and wearable electronics, such as health/wellness monitors, body sensor networks, and artificial muscles, contribute greatly to the development of human interactive applications.[1–11] These products can expediently capture the human physiological or behavioral characteristics and protect people's health, simultaneously have no harm or discomfort for people. For example, monitoring the body temperature and blood pressure of people can help them find the sign of getting sick,[6] capturing the body motions is beneficial for the sport training.[8] However, a key constraint of the rapid development of wearable electronics lies in their dependence on external sources, like battery or supercapacitor which is demanded to be charged before its exhaustion.[12–15] Whereupon, building a self-powered system is becoming a vital step to boost the development of wearable human interactive system. Recently, the integration of wearable electronics with flexible generators based on piezoelectric or electrostatic effect may give a strategy to overcome power supply challenges.[2,3,16–23] Those generators could also act as an active sensor except for the advantage in converting motion into electric signals.[19,21,22]

However, fragile inorganic piezoelectric materials, such as lead zirconate titanate (PZT)[16] and lead magnesio-niobate titanate (PMN-PT),[17] contain the lead element, which carries potential health risks. The piezoelectric property of flexible organic piezoelectric materials, such as polyvinylidene fluoride (PVDF),[18] is not excellent enough for practical applications. Traditional flexible triboelectric generators and electrostatic generators go against to assemble with human body well.[20–25] Though, single electrode triboelectric generators are proposed to address the issue significantly, the exposed residual charges of generators are easy to lose.[26,27] Consequently, new strategy should be proposed to develop other kind of flexible generators to sustainably power the wearable electronic systems. Cellular polypropylene piezoelectret, which is flexible, light-weight, inexpensive, and has the similar property with traditional piezoelectric materials,[28–30] was first proposed by Kari Kirjavainen and co-workers in 1990.[31] In the past 25 years, cellular polypropylene has been applied in many transducer applications, like loudspeakers and energy harvesters, because of its rather small specific acoustic impedance and relative high piezoelectric coefficient (d_{33}).[32–35]

Herein, we present a new type of flexible generator based on cellular polypropylene piezoelectret. By virtue of the outstanding mechanical property and high d_{33}, the simple-structured cellular polypropylene piezoelectret flexible generator (CPPFG) can efficiently transfer the mechanical energy into electrical power and possesses long-term stable output performance, reaching the peak power density of ≈52.8 mW m^{-2}. For wearable and human interactive applications, self-powered human body biological signals detecting sensors that can sensitively measure the coughing action and arterial pulses were demonstrated, indicating the potential application in healthy monitoring. This study develops a new and efficient path for human body energy harvesting and interactive sensing.

2. Results and Discussion

The fabrication process began with the low-cost and easy-gotten biaxially oriented multilayer polypropylene film (Treofan film EUH75). The detailed process is schematically provided in **Figure 1**a. The multilayer polypropylene film was first put into a chamber with the chamber pressure of 2 MPa and temperature of 100 °C for 3 h, following by a quick deflation process.

N. Wu, X. Cheng, Q. Zhong, J. Zhong, W. Li, B. Wang, Dr. B. Hu, Prof. J. Zhou
Wuhan National Laboratory for Optoelectronics and School of Optical and Electronic Information
Huazhong University of Science and Technology
Wuhan 430074, China
E-mail: jun.zhou@mail.hust.edu.cn

DOI: 10.1002/adfm.201501695

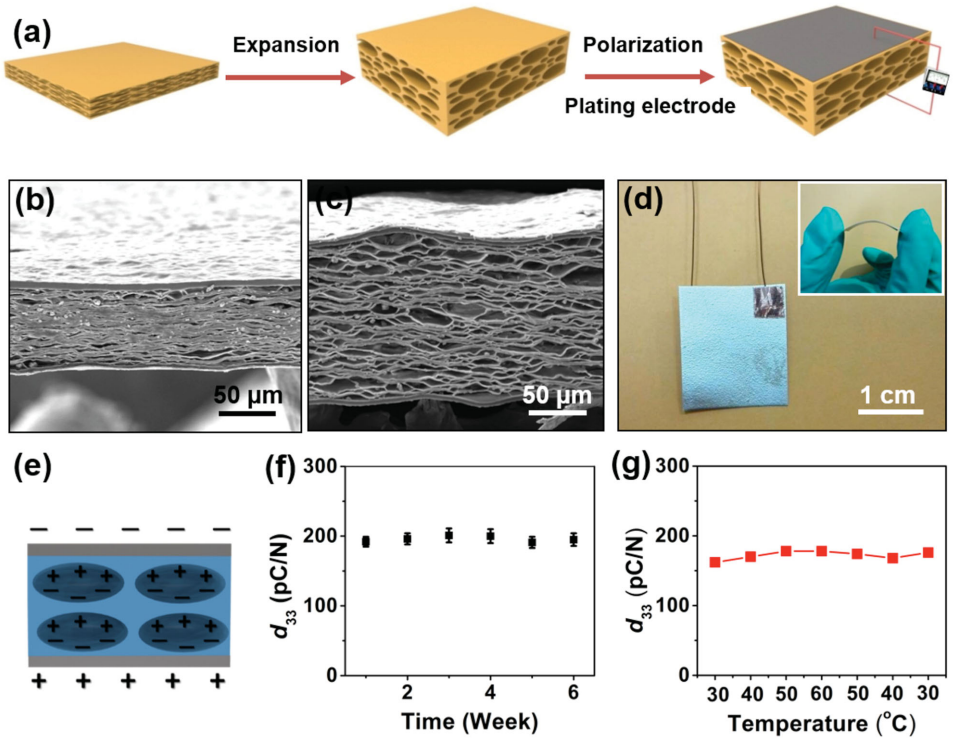

Figure 1. Fabrication process and physical performance of a CPPFG. a) The schematic diagram illustrating the fabrication process. Cross-section view scanning electron microscope (SEM) images of the cellular polypropylene b) before and c) after expanding. d) Digital picture showing a CPPFG, inset indicates the flexibility of the CPPFG. e) Schematic model of charge distribution in the cellular polypropylene. The d_{33} values for the samples f) placed for weeks and g) worked under different environment temperature from 30 to 60 °C.

As a result, the thickness of polypropylene film expands from original ≈75 μm to ≈150 μm, as shown in Figure 1b,c. It can be seen in Figure 1c that oval air bubbles with diameter of tens micrometer are formed, making the common multilayer polypropylene film be the functional cellular polypropylene film. Then, the expanded polypropylene film was charged by applying a high voltage to it. Subsequently, magnetron sputtering system was used to metallize samples with sliver on both sides. The digital picture of the device is shown in Figure 1d and the inset picture demonstrates the excellent flexibility of the generator.

The detailed high voltage charging device is schematically indicated in Figure S1, Supporting Information. A high voltage of −16 kV was applied to the cellular polypropylene for 3 min, with the samples placed 5 cm below the corona needle. As a result, the air in the air bubbles is ionized and broken down, generating charges with opposite polarity on both sides of the air bubbles. Simultaneously, corresponding induced charges will form in the electrodes, as indicated in Figure 1e. In the charged cellular polypropylene, all bubbles with charged internal surface work as electric dipole. The large number of bubbles yields amazingly high d_{33} value.[28,30]

In our study, the d_{33} value of cellular polypropylene is significantly affected by the detailed expansion conditions, including expansion temperature and chamber pressure. For a given expansion chamber pressure (2 MPa), the d_{33} value increased with the expansion temperature (Figure S2a, Supporting Information). However, if the expansion temperature was over 100 °C, the samples would start to melt. On the other hand, the d_{33} value also increased by increasing the expansion chamber pressure under a constant expansion temperature (100 °C). Nevertheless, the d_{33} value increased slowly when the expansion chamber pressure was over 2 MPa (Figure S2b, Supporting Information). As a result, chamber pressure of 2 MPa and temperature of 100 °C are selected as the optimized expansion condition. The d_{33} value of the original multilayer polypropylene was only 19 pC N^{-1} in average, but it was 205 pC N^{-1} in average for the expanded cellular polypropylene, almost the same large as the commercial PZT, as shown in Table 1, Supporting Information. The remarkable stability of the cellular polypropylene is also proved. The d_{33} value for cellular polypropylene which was placed for weeks almost kept at ≈200 pC N^{-1} (Figure 1f). Simultaneously, the cellular polypropylene performs stability below 60 °C and has the repeatability, as shown in Figure 1g, but the d_{33} values quickly drop by raising the temperature over 60 °C (Figure S2c, Supporting Information).

The ideal and simplified cellular polypropylene model is shown in Figure S3, Supporting Information. The cellular polypropylene film can be simplified as polypropylene-air-polypropylene sandwich structure, in which there are n layers of air and n+1 layers of polypropylene. After the high voltage charging process, the top and bottom surface of each air layer is charged with equal amounts of heterogeneous charge density $-\sigma_n$ and σ_n separately. Here we define the electric field E direction from the bottom to the top as the positive direction. According to Gauss law, then for any layer i ($1 \le i \le n$)

$$\varepsilon E_{1i} - E_{2i} = -\frac{\sigma_i}{\varepsilon_0} \quad (1)$$

$$E_{2i} - \varepsilon E_{1(i+1)} = \frac{\sigma_i}{\varepsilon_0} \quad (2)$$

where ε_0 and ε are the dielectric constant of air and relative dielectric constant of polypropylene, respectively. E_{1i} and E_{2i} represent the electric field of corresponding layer i. Combining Equations (1) and (2), we can find that $E_{11} = ... = E_{1i} = ... = E_{1n}$. According to Kirchhoff's second law under the short-circuit condition

$$\sum_{i=1}^{n+1} d_{1i} E_{1i} + \sum_{i=1}^{n} d_{2i} E_{2i} = 0 \quad (3)$$

where d_{1i} and d_{2i} represent the thickness of polypropylene and air layer, respectively. To simplify the mathematical analysis, we assume that each air layer has the same thickness, $d_2 = d_{2i}$ in the schematic diagram. Then the electric field of polypropylene layer E_{1i} can be expressed as

$$E_{1i} = -\frac{D_2 \sum_{i=1}^{n} \sigma_i}{n\varepsilon_0 (D_1 + \varepsilon D_2)} \quad (4)$$

where D_1 and D_2 are the total thickness of polypropylene and air layer, respectively:

$$D_1 = \sum_{i=1}^{n+1} d_{1i} \quad D_2 = \sum_{i=1}^{n} d_{2i} \quad (5)$$

As a result, the charge density on the electrode σ_0 can be given by

$$\sigma_0 = -\varepsilon_0 \varepsilon E_{1i} = \frac{\varepsilon \sum_{i=1}^{n} \sigma_i}{n\left(\frac{D_1}{D_2} + \varepsilon\right)} \quad (6)$$

Figure 2a schematically indicates the power generating process of a CPPFG. As shown in Figure 2a-I, the charge density on the electrode σ_0 is decided by the above equation, in the original state. When the CPPFG is pressed, the total thickness of air layers D_2 will be reduced, resulting in a decreasing of the charge density on the top and bottom electrodes. As a result, the current will flow from bottom electrode to the top electrode and an instantaneous positive current signal will be noticed, as shown in Figure 2a-II. With the compression increased, the charge density on both electrodes will continually decrease until a new equilibrium is established, as illustrated in Figure 2a-III. In the releasing process, the generator will return back to its original shape and the total thickness of air layers D_2 increases. The charge density on both electrodes will also increase, leading to current flowing back from top electrode to the bottom electrode and an instantaneous negative current signal will be noticed, as shown in Figure 2a-IV.

In general, the variation of charge density on CPPFG electrodes will lead to alternating currents through the external circuit, which is shown in Figure 2b. Switching polarity tests were also carried out to confirm that the measured output signals are generated from the generator rather than from the measurement system (Figure 2c). To rule out the possible artifacts, the short circuit output current and open circuit output voltage for two CPPFG connected in parallel were measured and the results are shown in Figure 2d,e. When two CPPFG were connected in the same direction, the total output current and voltage increased. When two CPPFG were connected in antiparallel, the total output current and voltage weakened. The results indicate that the output properties of the CPPFG satisfy linear superposition criterion in the basic circuit connections.

The electrical performances of a CPPFG were systematically studied by regularly stimulated by a linear motor. Specifically, a CPPFG, with effective area of 17.5 mm^2, was fixed and periodically pressed and released under different stimulated force and frequency, as shown in Figure S4, Supporting Information.

In order to find out the peak power density, the output performances under different external load were measured at a

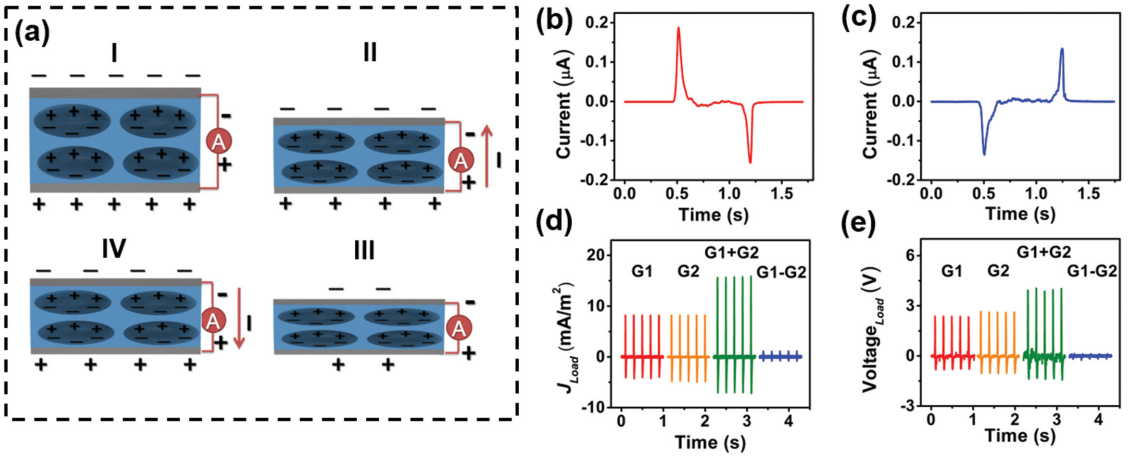

Figure 2. Working mechanism of a CPPFG. a) Schematic diagram indicates the working mechanism of a CPPFG when it is at (I) the original, (II) the pressing, (III) the equilibrium, and (IV) the releasing states, respectively. Short-circuit currents for the CPPFG when it is b) forward-connected and c) reverse-connected to the measurement system, respectively. d) Short-circuit currents and e) open-circuit voltages for two CPPFG when they are in parallel and reverse parallel connection, respectively.

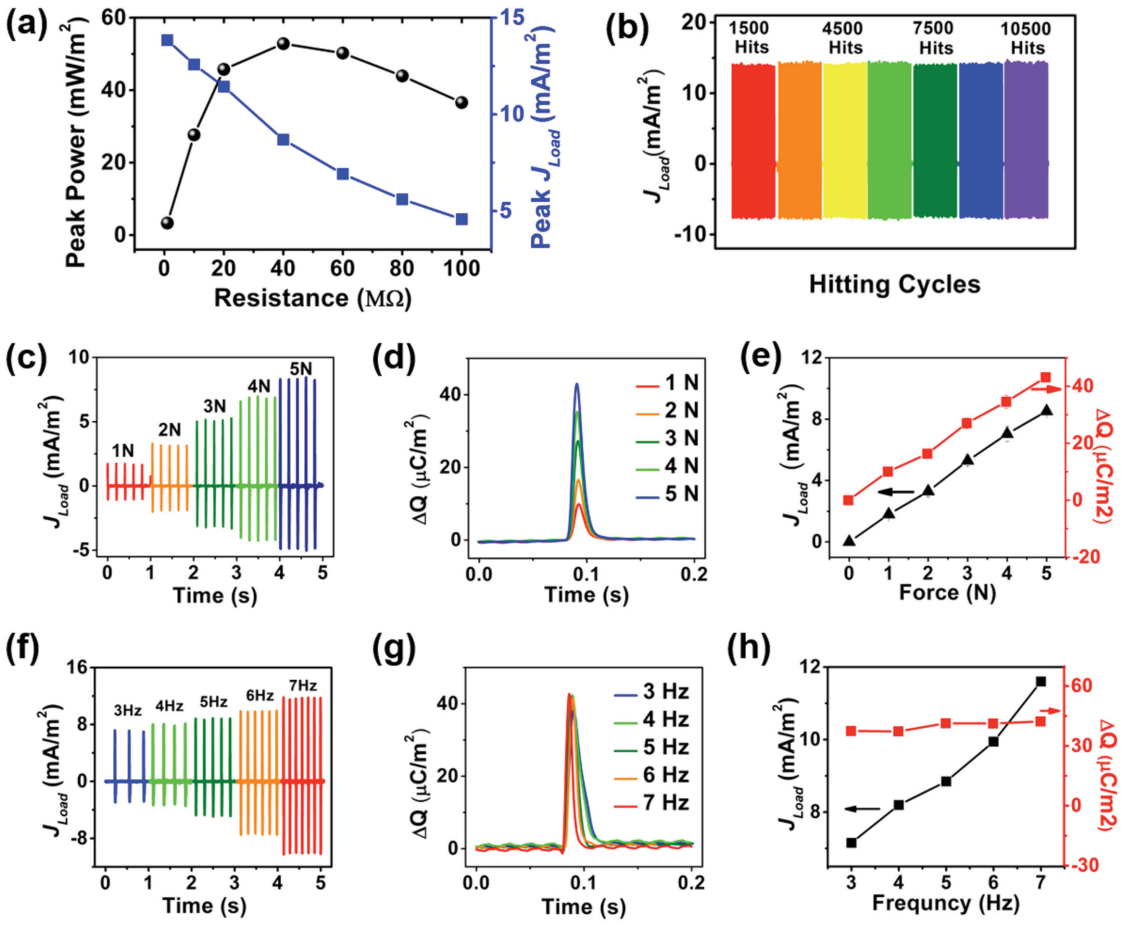

Figure 3. Performance of a CPPFG. a) Peak output currents and power density of a CPPFG with different external loads. b) Output current–time curves for ≈10 500 cycles continuous working of a CPPFG. c) Loading current–time curves, d) corresponding transferred charges–time curves and e) peak values for loading currents and transferred charges for a CPPFG stimulated at different force and a given frequency of 5 Hz. f) Loading current–time curves, g) corresponding transferred charges–time curves, and h) peak values for loading currents and transferred charges for a CPPFG stimulated at different frequencies under a given force of 5 N.

stimulated frequency of 5 Hz and force of 5 N, as indicated in **Figure 3**a. It can be seen that the load peak current density decreased, from ≈13.8 mA m^{-2} at 1 MΩ to ≈4.6 mA m^{-2} at 100 MΩ, as the external load resistance increased step by step. According to the power definition: $P = I^2R$, a maximum output peak power density of ≈52.8 mW m^{-2} was obtained for a corresponding load of 40 MΩ. The stability of the output performance of a CPPFG is excellent. In this work, the CPPFG was continuously hit for ≈10 500 cycles at a stimulated force of 5 N and frequency of 5 Hz. The outputs for different stimulated cycles are shown in Figure 3b, indicating the ignorable variation. Meanwhile, no noticeable morphology degradation of the CPPFG after the long-term test was found from the SEM analysis (Figure S5, Supporting Information).

The load peak current density and the corresponding total amount integral transferred charges of a CPPFG increased approximately linearly as the stimulated force increasing, from ≈1.8 mA m^{-2} and ≈10.0 μC m^{-2} at 1 N to ≈8.5 mA m^{-2} and ≈43.1 μC m^{-2} at 5 N, for a given frequency of 5 Hz and load resistance of 40 MΩ, as shown in Figure 3c–e. On the other hand, for a constant stimulated force of 5 N and vibrational frequencies from 3 to 7 Hz, the load peak current density increased step by step too, from ≈7.2 mA m^{-2} at 3 Hz to ≈11.6 mA m^{-2} at 7 Hz (Figure 3f). However, the total amount integral transferred charges kept almost the same, with the value of ≈41.0 μC m^{-2} (Figure 3g,h). According to above results, increasing the stimulated force and frequency can lead to the larger peak current density, but the total amount integral transferred charges is only related to the stimulated force.

Inspired from the emergence of human personalized healthcare basing on wearable electronics, here we introduced human body biological signals detecting sensors based on the CPPFG to measure the vocal cords vibration and arterial pulses. As illustrated in **Figure 4**a, the sensor was fastened on a healthy young man neck, and then the current signals were generated by coughing through vocal cords vibration, as shown in Figure 4b and Video 1. The enlarged view of the current signal generated by one coughing action is recorded in Figure 4c. In order to validate the current signals truly generated from vocal cords vibration, the power spectrum of the current signal in Figure 4c basing on fast Fourier transform (FFT) is presented

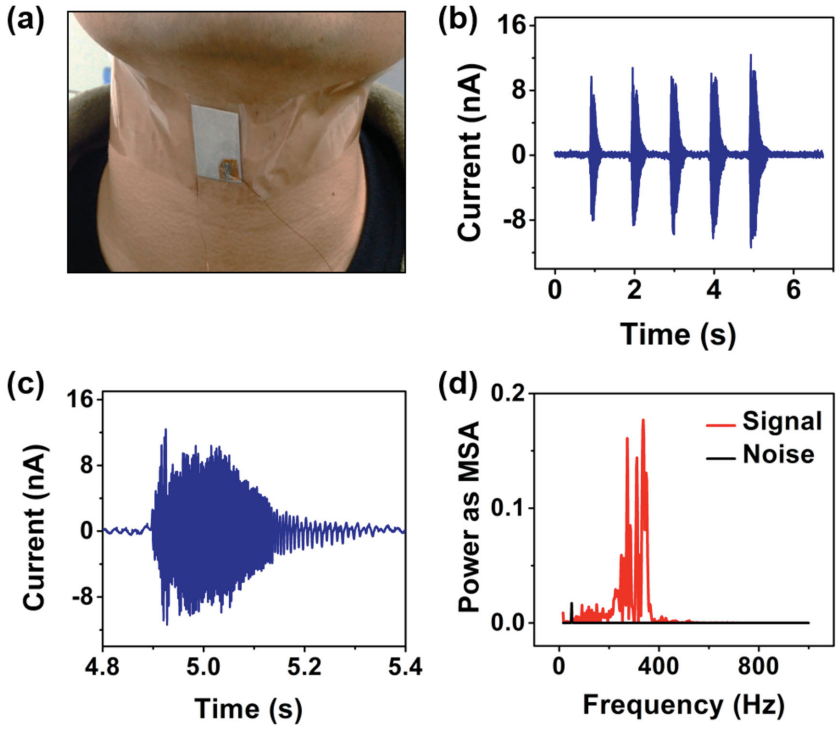

Figure 4. A human body biological signals detecting sensor to measure the coughing action. a) Digital picture of a sensing system. b) The current–time curves for the sensor caused by coughing. c) The enlarged view of the current signal generated by one coughing action. d) Fast Fourier transforms for the current signals and the base noise, respectively.

in Figure 4d, and the power spectrum density is normalized by mean square amplitude method (MSA). The result shows that frequency band in signal covers 250–400 Hz, which has the same frequency characteristics of healthy people coughing sound.[36,37] Meanwhile, the power spectrum of a same-length signal without coughing indicates that the amplitude or energy of background noise is much smaller, which reveals the power spectrum of the coughing signal is not influenced by background noises.

On the other hand, the sensor was also fastened on the wrist to detect the arterial pulses of a young man, as shown in **Figure 5**a and Video 2. Figure 5b represents the enlarged view of one cycle of the current signal. The waveform is composed of five main parts, labeled as initially positive (A-wave), early negative (B-wave), reincreasing (C-wave), late redecreasing (D-wave), and diastolic positive (E-wave), clearly showing the details of a heartbeat.[38] The heartbeat times of this man at ordinary state recorded by our sensor is ≈78 times min^{-1} (Figure 5c), which is accorded with the normal times of healthy young mans, the number of 60 to 100 times min^{-1}. After this man having run for 5 min, his heartbeat times went up to ≈108 times min^{-1} (Figure 5d). Meanwhile, the sensor was also fastened on the arm where there was no arterial pulses, in order to exclude other interference signals. No obvious and regular current signals were recorded, as shown in Figure S6, Supporting Information. According to above discussion, the human body biological signals detecting sensors may have potential application in self-powered human healthy monitoring, paving a new developing way for self-powered wearable electronics.

3. Conclusions

In conclusion, we introduce the unique, simple-structured, and efficient human body energy harvesting and self-powered human interactive sensing systems based on the cellular polypropylene piezoelectret and electrostatic induction effect. The CPPFG showed stable and excellent output performance, with maximum peak power density of ≈52.8 mW m^{-2}. Meanwhile, the detailed power generating mechanism was systematically explored. For wearable and health monitoring application, self-powered human body biological signals detecting sensors were proved, which could sensitively detect the coughing action and arterial pulses. The new way and process proposed in this study will help to instigate the development of wearable electronics, aiming for building the self-powered healthy monitoring and interactive sensing systems.

4. Experimental Section

Expansion of Cellular Polypropylene: The biaxially oriented multilayer cellular polypropylene films (Treofan film EUH75) were used as the raw material. These films were first cut into 6 × 6 cm samples. These samples were placed into the chamber afterwards and exposed to nitrogen gas at the gas pressure of 2 MPa and temperature of 100 °C for 3 h to equalize the gas pressure between the cellular and the chamber. Then the gas pressure of the chamber was quickly deflated to atmospheric pressure within 5 s and samples were taken from the chamber. During this process, the thickness of cellular polypropylene films can be doubled from original ≈75 to ≈150 μm.

Fabrication Process of CPPFG: The fabrication process began with the corona charging process. The charging system was made up of a negative high voltage DC power supply and a corona needle. When charging, samples were placed 5 cm below the corona needle and needle voltage was maintained at −16 kV for 3 min. Subsequently, magnetron sputtering system was used to metallize samples with sliver on both sides.

Measurement of d_{33} Value: The piezoelectric coefficient d_{33} (C/N) quantifies the change of the transferred charges when a vertical force is applied to the device. Its first and second subscripts represent the direction of electric field and applied force, respectively. In our test, our device was fixed and stimulated at a frequency of 5 Hz and force of 5 N under the short-circuit condition. During this process, an instantaneous positive and negative current would be noticed in one period. Then we could calculate the transferred charges by integrating the positive or the negative current peak. The piezoelectric coefficient d_{33} can be calculated by the following equation

$$d_{33} = Q/F \tag{7}$$

where Q is the transferred charges and F is the applied vertical force.

Characterization: The morphology of samples is probed by a high-resolution field emission scanning electron microscope (FEI Nova NanoSEM 450). The voltage and current output of the samples are measured by KEITHLEY 6514 meter and a Stanford low-noise current

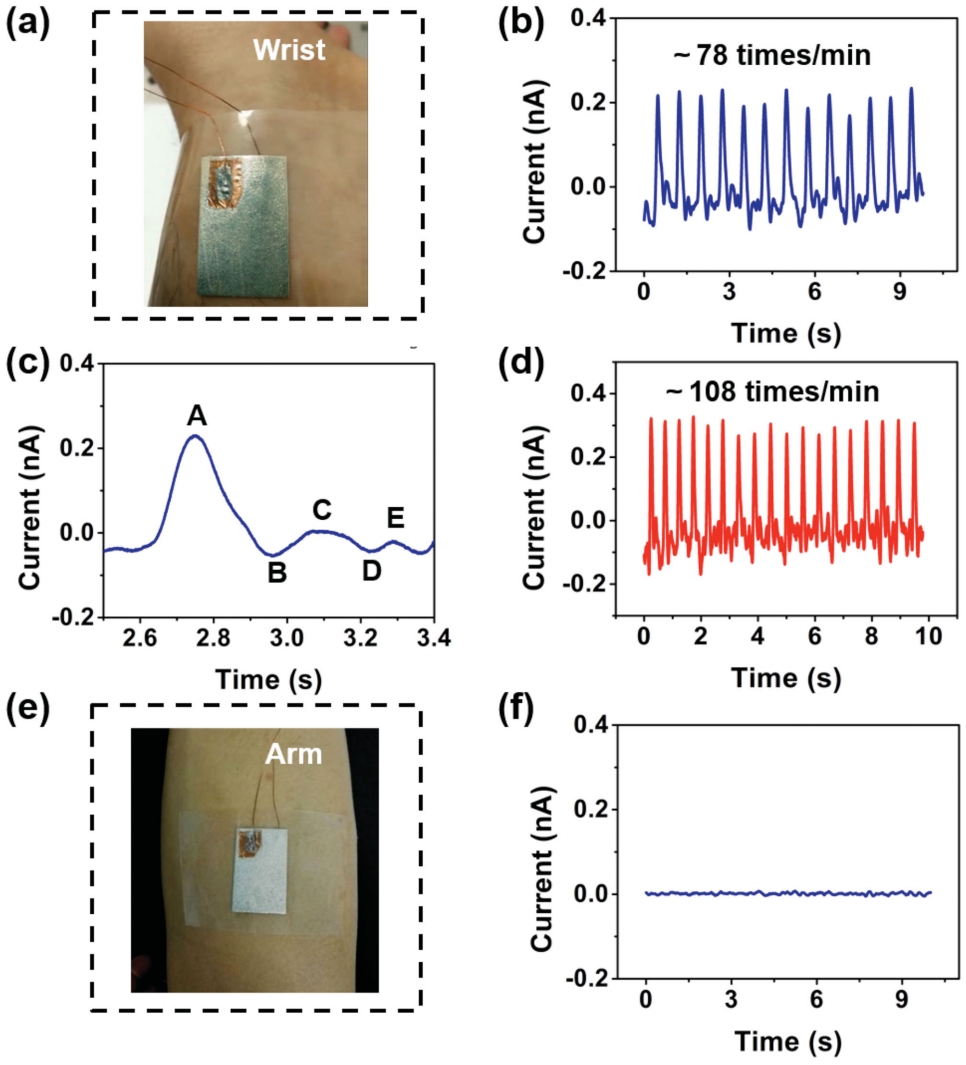

Figure 5. A human body biological signals detecting sensor to measure the arterial pulses. a) Digital picture of a sensor fastened on the wrist. b) The current–time curves for the sensor stimulated by the arterial pulses of a young man at ordinary state. c) The enlarged view of one cycle of the current signal. d) The current–time curves for the sensor stimulated by the arterial pulses of a young man after running for 5 min. e) Digital picture and f) the current–time curve of a sensor fastened on the arm.

preamplifier (Model SR570), respectively. These data are acquired by NI PCI-6259. The corona polarization method is carried out with DW-N503-4ACDE high voltage source.

Supporting Information

Supporting Information is available from the Wiley Online Library or from the author.

Acknowledgements

N.W. and X.C. contributed equally to this work. This work was financially supported by the National Natural Science Foundation of China (51322210, 61434001) and Director Fund of WNLO. The authors thank to the facility support of the Center for Nanoscale Characterization & Devices, WNLO-HUST, and the Analysis and Testing Center of Huazhong University of Science and Technology.

Received: April 27, 2015
Revised: May 26, 2015
Published online: June 24, 2015

[1] L. C. Rome, L. Flynn, E. M. Goldman, T. D. Yoo, *Science* **2005**, *309*, 1725.
[2] Z. L. Wang, J. Song, *Science* **2006**, *312*, 242.
[3] L. Persano, C. Dagdeviren, Y. Su, Y. Zhang, S. Girardo, D. Pisignano, Y. Huang, J. A. Rogers, *Nat. Commun.* **2013**, *4*, 1633.
[4] W. Zeng, L. Shu, Q. Li, S. Chen, F. Wang, X.-M. Tao, *Adv. Mater.* **2014**, *26*, 5310.
[5] C. Sun, J. Shi, D. J. Bayerl, X. Wang, *Energy Environ. Sci.* **2011**, *4*, 4508.
[6] J. Zhong, Y. Zhang, Q. Zhong, Q. Hu, B. Hu, Z. L. Wang, J. Zhou, *ACS Nano* **2014**, *8*, 6273.

[7] J. A. Rogers, *Nature* **2010**, *468*, 177.
[8] T. Yamada, Y. Hayamizu, Y. Yamamoto, Y. Yomogida, A. Izadi-Najafabadi, D. N. Futaba, K. Hata, *Nat. Nanotechnol.* **2011**, *6*, 296.
[9] C. Wang, D. Hwang, Z. Yu, K. Takei, J. Park, T. Chen, B. Ma, A. Javey, *Nat. Mater.* **2013**, *12*, 899.
[10] D. J. Lipomi, M. Vosgueritchian, B. C. K. Tee, S. L. Hellstrom, J. A. Lee, C. H. Fox, Z. Bao, *Nat. Nanotechnol.* **2011**, *6*, 788.
[11] P. Needham, L. Gamlyn, in *Proc. 1st Int. Workshop Wearable Implantable Body Sensor Network,* London, UK **2004**, 49–50.
[12] Y.-H. Lee, J.-S. Kim, J. Noh, I. Lee, H. J. Kim, S. Choi, J. Seo, S. Jeon, T.-S. Kim, J.-Y. Lee, J. W. Choi, *Nano Lett.* **2013**, *13*, 5753.
[13] L. Hu, M. Pasta, F. L. Mantia, L. Cui, S. Jeong, H. D. Deshazer, J. W. Choi, S. M. Han, Y. Cui, *Nano Lett.* **2010**, *10*, 708.
[14] J. A. Lee, M. K. Shin, S. H. Kim, H. U. Cho, G. M. Spinks, G. G. Wallace, M. D. Lima, X. Lepró, M. E. Kozlov, R. H. Baughman, S. J. Kim, *Nat. Commun.* **2013**, *4*, 1970.
[15] X. Xiao, T. Li, P. Yang, Y. Gao, H. Jin, W. Ni, W. Zhan, X. Zhang, Y. Cao, J. Zhong, L. Gong, W.-C. Yen, W. Mai, J. Chen, K. Huo, Y.-L. Chueh, Z. L. Wang, J. Zhou, *ACS Nano* **2012**, *6*, 9200.
[16] S. Xu, B. J. Hansen, Z. L. Wang, *Nat. Commun.* **2010**, *1*, 93.
[17] G.-T. Hwang, H. Park, J.-H. Lee, S. Oh, K.-I. Park, M. Byun, H. Park, G. Ahn, C. K. Jeong, K. No, H. Kwon, S.-G. Lee, B. Joung, K. J. Lee, *Adv. Mater.* **2014**, *26*, 4880.
[18] C. Chang, V. H. Tran, J. Wang, Y.-K. Fuh, L. Lin, *Nano Lett.* **2010**, *10*, 726.
[19] S. Lee, S.-H. Bae, L. Lin, Y. Yang, C. Park, S.-W. Kim, S. N. Cha, H. Kim, Y. J. Park, Z. L. Wang, *Adv. Funct. Mater.* **2013**, *23*, 2445.
[20] F.-R. Fan, Z.-Q. Tian, Z. L. Wang, *Nano Energy* **2012**, *1*, 328.
[21] Q. Zhong, J. Zhong, B. Hu, Q. Hu, J. Zhou, Z. L. Wang, *Energy Environ. Sci.* **2013**, *6*, 1779.
[22] B. Hu, W. Chen, J. Zhou, *Sensors Actuators B-Chem.* **2013**, *176*, 522.
[23] G. Zhu, J. Chen, T. Zhang, Q. Jing, Z. L. Wang, *Nat. Commun.* **2014**, *5*, 3426.
[24] J. Zhong, Q. Zhong, F. Fan, Y. Zhang, S. Wang, B. Hu, Z. L. Wang, J. Zhou, *Nano Energy* **2013**, *2*, 491.
[25] X.-S. Zhang, M.-D. Han, R.-X. Wang, F.-Y. Zhu, Z.-H. Li, W. Wang, H.-X. Zhang, *Nano Lett.* **2013**, *13*, 1168.
[26] B. Meng, W. Tang, Z.-H. Too, X. Zhang, M. Han, W. Liu, H. Zhang, *Energy Environ. Sci.* **2013**, *6*, 3235.
[27] Y. Yang, H. Zhang, J. Chen, Q. Jing, Y. S. Zhou, X. Wen, Z. L. Wang, *ACS Nano* **2013**, *7*, 7342.
[28] X. Zhang, J. Huang, J. Chen, Z. Wan, S. Wang, Z. Xia, *Appl. Phys. Lett.* **2007**, *91*, 182901.
[29] G. M. Sessler, J. Hillenbrand, *Appl. Phys. Lett.* **1999**, *75*, 3405.
[30] X. Zhang, J. Hillenbrand, G. M. Sessler, *J. Phys. D: Appl. Phys.* **2004**, *37*, 2146.
[31] A. S avolainen, K. Kirjavainen, *J. Macromol. Sci. Chem.* **1989**, *26*, 83.
[32] W. Jhih-Jhe, H. Tsung-Hsing, Y. Che-Nan, T. Jui-Wei, S. Yu-Chuan, *J. Micromech. Microengin.* **2012**, *22*, 015013.
[33] Y. Feng, K. Hagiwara, Y. Iguchi, Y. Suzuki, *Appl. Phys. Lett.* **2012**, *100*, 262901.
[34] J. Hillenbrand, G. M. Sessler, *Ferroelectrics* **2014**, *472*, 77.
[35] S. Anton, K. Farinholt, A. Erturk, *J. Intel. Mat. Syst. Str.* **2014**, *25*, 1681.
[36] J. Korpáš, J. Sadloňová, M. Vrabec, *Pulmonary Pharmacol.* **1996**, *9*, 261.
[37] S. Leconte, G. Liistro, P. Lebecque, J. Degryse, *Eur. Respir. J.* **1995**, *8*, 1949.
[38] J. Yang, J. Chen, Y. Su, Q. Jing, Z. Li, F. Yi, X. Wen, Z. Wang, Z. L. Wang, *Adv. Mater.* **2015**, *27*, 1316.